Available online at www.sciencedirect.com

ScienceDirect

Procedia Structural Integrity 80 (2026) 321–326

Structural Integrity Procedia

www.elsevier.com/locate/procedia

Fracture, Damage and Structural Health Monitoring

Damage Index Selection For Ultrasonic Guided Waves Based Structural Health Monitoring System

Antonio Polverino[a]*, Donato Perfetto[a], Francesco Caputo[a] , Dimitrios Zarouchas[b], Alessandro De Luca[a]

[a]*Department of Engineering, University of Campania "L. Vanvitelli", 81031, Via Roma 29, Aversa, Italy*
[b]*Center of Excellence in AI for Structures, Prognostics & Health Management, Aerospace Engineering Faculty, Delft University of Technology, Kluyverweg 1, Delft, 2629 HS, The Netherlands*

Abstract

Ultrasonic Guided Waves (UGW) are widely used in Structural Health Monitoring (SHM) due to their ability to inspect large areas with minimal sensor instrumentation. However, the acquired signals can be challenging to interpret, as they are highly sensitive to material properties, environmental factors and operating conditions. To enhance interpretability and comparability, simplifying these signals into dimensionless quantities is crucial. This study employs finite element (FE) method to model cracks in a thin aluminum panel, aiming to identify the most effective post-processing technique for UGW signals acquired by a network of piezoelectric sensors distributed across the panel's surface. Damage indicators in both the frequency and time domains are evaluated based on their correlation with critical crack parameters, such as position and size. The findings contribute to optimizing monitoring techniques for timely and accurate damage diagnosis in thin structures, offering valuable insights for predictive maintenance in SHM applications.

Keywords: SHM; UGW; FEM.

1. Introduction

SHM plays a fundamental role in ensuring the safety and integrity of critical structures in aerospace, mechanical,

* Corresponding author.
E-mail address: Antonio.Polverino@unicampania.it

10.1016/j.prostr.2026.02.031

and civil applications. Among the available non-destructive evaluation techniques, UGW have gained significant traction due to their ability to propagate over long distances and interact sensitively with structural discontinuities (Su & Ye, 2009). This allows the inspection of large surfaces with a relatively small number of sensors, making UGW-based systems both cost-effective and efficient. However, since the interpretation of UGW signals remains a complex task, to enhance their interpretability, they are often post-processed into simplified, dimensionless quantities known as Damage Indices (DIs). These indices are calculated by comparing signals acquired in a damaged state with a baseline from the pristine condition. Despite their widespread use, DIs present some limitations. Their effectiveness can vary significantly depending on a wide range of factors, including material properties, structural geometry, damage type, and environmental conditions (Konstantinidis et al., 2006). This variability makes it difficult to generalize their use across different scenarios. As a result, selecting an appropriate DI is often empirical, and there remains a need to better understand which perform best under specific conditions. Recently, FE modelling has proven to be a powerful tool for simulating UGW propagation and their interaction with structural defects (Özgan et al., 2024) allowing the systematic study of wave behavior under varying damage configurations, material conditions, or sensor layouts. In this work, FE models of a thin aluminum panel with varying crack lengths and positions is used to evaluate eight different DIs consequently assessed based on their sensitivity to the presence and evolution of a crack. The evaluation framework focuses on two key characteristics: the correlation between each DI and the crack length, and the spatial coherence of each DI in relation to the crack's proximity to the receivers quantified through the *Length Effectiveness Score (LES)* and the *Position Effectiveness Score (PES)*, respectively. Through this study, the authors offers a more rigorous basis for selecting and interpreting Dis in UGW-based SHM systems, helping for diagnostic strategies to specific structural and damage conditions.

Nomenclature

DI	Damage Index
FE	Finite Element
LES	Length Effectiveness Score
SHM	Structural Health Monitoring
PES	Position Effectiveness Score
PZT	Lead Zirconate Titanite
UGW	Ultrasonic Guided Waves

2. Methodology

In this study, an aluminum alloy panel (Al 2024-T3), schematized in Fig. 1, was considered as a case study. A FE model was developed using Abaqus® Explicit, simulating the generation and propagation of UGW induced and acquired by Lead Zirconate Titanite (PZT) transducers. To isolate the effects of damage and avoid edge reflections, the panel was modelled as an infinite plate by incorporating absorbing elements at the boundaries (CIN3D8), thereby eliminating wave reflections and simplifying wave interpretation. The modelled plate consists of C3D8R elements with an average element size of 0.75 mm, ensuring a spatial resolution of 20 nodes per wavelength. Five PIC255 PZT transducers were surface-mounted: one at the center acting as an actuator, and four placed symmetrically around it as receivers, forming a square of side $L = 140$ mm. Each PZT sensor has a diameter of 10 mm and a thickness of 0.2 mm. The transducers were integrated into the mesh using node-to-surface constraints, without explicitly modelling the bonding layer (justified by previous literature (De Luca et al., 2022)). The FE mesh count 143,000 nodes and 430,000 degrees of freedom, providing high fidelity in simulating wave propagation. The actuator was excited using a five-cycle Hanning-windowed tone burst cantered at 200 kHz, chosen to excite only the fundamental UGW modes (S_0 and A_0), thereby avoiding the complexity introduced by higher-order modes. The equivalent radial displacement, Calculated as descripted in (De Luca et al., 2021), was applied on the nodes of the upper circumference of the actuator. A total simulation time of 100 μs with a time step of 120 ns was used, selected considering the wave speed and the minimum element length to satisfy the stability condition. A total of 80 crack positions (schematized as black crosses in Fig. 1) were evaluated by varying the crack center in a grid from -80 mm to +80 mm along both the X and Y directions (step of 20 mm), excluding the central position, already occupied from the actuator sensor. For each position, 10 crack lengths (from 1.5 mm to 15 mm, in steps of 1.5 mm) were analyzed for a total of 800 crack configuration. To simulate a through-thickness crack-induced scattering, the damage was

introduced by modelling a seam at the interface of the involved finite elements simulating a physical crack. For each damage scenario, the UGW response was acquired from all four receivers by averaging the in-plane logarithmic strains across the elements representing each PZT. The list of the evaluated DIs, extracted from literature, is reported in Table 1, and includes indices in both time and frequency domains: A_p and A_d are the amplitudes of direct S_0 mode wave packet captured in pristine and damaged configuration, respectively; $\bar{p}$ and $\bar{d}$ are the means of the signal captured in pristine and damaged configuration, respectively, both equal to 0; p_i and d_i are the amplitudes of the i-th sample point of the signal captured in pristine and damaged configuration, respectively; F_i^I and F_i^{II} are the amplitude of the i-th frequency components of the complete frequency spectrum of the signal captured in pristine and damaged configuration, respectively. F_{max}^I and F_{max}^{II} represent the amplitudes of maximum frequency component in pristine and damaged configuration respectively. To quantitatively assess the effectiveness of each DI, two metrics were introduced. The *Length Effectiveness Score (LES)* quantifies the monotonic relationship between the values of a DI and the crack length. It is computed as the coefficient of determination (R^2) between the *i*-th DI, averaged over all analyzed crack positions, and the crack length (l), as shown in Equation 1. The *Position Effectiveness Score (PES)* evaluates how coherently each DI responds to the spatial proximity of the damage to the receivers ($r = 1, 2, 3, 4$). It is calculated as the absolute value of the Pearson correlation between the *i*-th DI, averaged over all crack lengths, and the inverse distance to the respective receivers, as described in Equation 2. A high LES value indicates a strong monotonic relationship between the index and the crack length, while a high PES value indicates that the DI responds coherently with spatial proximity to the sensors, highlighting its physical sensitivity to the damage location.

$$LES_i = R^2(DI_i(l), l) \tag{1}$$

$$PES_i = \frac{\sum_{r=1}^{4} \left| corr\left(DI_i(p), \frac{1}{d_r(p)}\right) \right|}{4} \tag{2}$$

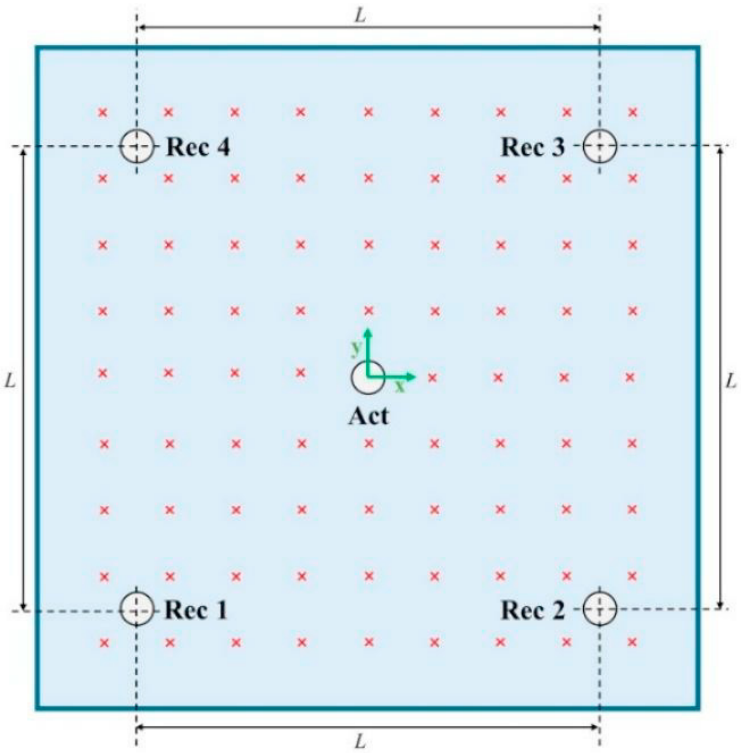

Fig. 1. Schematic of the case study and modeled crack position (red cross).

Table 1. Considered DIs.

formulae	Reference	Description
$DI_1 = \lvert(A_d - A_p)/A_p\rvert$	(Hu et al., 2022)	Relative variation rate of the amplitude of the direct wave between two signals acquired in different structural states.
$DI_2 = \left\lvert\frac{F^I_{max} - F^{II}_{max}}{F^I_{max}}\right\rvert$	(Hu et al., 2022)	Rate of variation of the maximum frequency component of the direct wave between two signals acquired in different structural states.
$DI_3 = 1 - \left(\frac{\sum_i (p_i - \bar{p})(d_i - \bar{d})}{\sqrt{\sum_i (p_i - \bar{p})^2 (d_i - \bar{d})^2}}\right)^2$	(Wu et al., 2021)	Relative variation rate of the amplitude of the wave at each time instance between two signals acquired in different structural states.
$DI_4 = \sqrt{\left\{\sum_i (p_i - d_i)^2 / p_i^2\right\}}$	(De Luca et al., 2023)	Normalized difference of the energy of the two signals acquired in different structural states.
$DI_5 = (A_p - A_d) \cdot (T_p - T_d)$	(Su & Ye, 2009)	Product of the difference in amplitude and the difference in the time of flight of the direct wave between two signals acquired in different structural states.
$DI_6 = 1 - \frac{\sum_i (p_i - \bar{p})(d_i - \bar{d})}{\sqrt{\sum_i (p_i - \bar{p})^2} \sqrt{\sum_i (d_i - \bar{d})^2}}$	(Su & Ye, 2009)	Relative variation rate of the amplitude of the wave at each time instance between two signals acquired in different structural states.
$DI_7 = \frac{\sum_{i=1}^N \lvert F_i^I - F_i^{II}\rvert}{\sum_{i=1}^N \lvert F_i^I\rvert}$	(Su & Ye, 2009)	Normalized difference of the signals in each frequency band between two different structural states.
$DI_8 = (T_d - T_p)/T_p$	(Wang et al., 2020)	Relative difference in the time of flight of the direct wave between two signals acquired in different structural states.

3. Results

To evaluate Dis effectiveness to both spatial position and crack growth, numerical results were analyzed with a focus on how their values evolve with increasing crack length and across different crack positions in relation to the receiver network. Fig. 2 presents the spatial sensitivity mapping of each DI. Each contour map shows values of a specific DI averaged over all crack lengths and receivers at each crack position. This visualization allows a qualitative assessment of how each index responds to crack placement. In particular, DI_2, DI_3, DI_4, DI_6, and DI_7 exhibit strong spatial coherence, where higher values appear in specific regions, suggesting a physically consistent response pattern. Fig. 3 displays the normalized values of all DIs as a function of crack length. This plot highlights the degree of monotonicity and sensitivity of each DI to crack growth. DI_6 shows an almost perfect linear trend, closely followed by DI_3, DI_7, DI_2, and DI_4, all exhibiting a consistent increase with crack length. These trends suggest that these indices are more suitable for damage progression tracking. Table 2 quantitatively summarizes the LES and PES for each considered DI. These findings demonstrate that not all DIs perform equally under the same conditions, and highlight the importance of selecting indices based on both the damage type and the desired diagnostic objective: crack localization, growth tracking, or general detection.

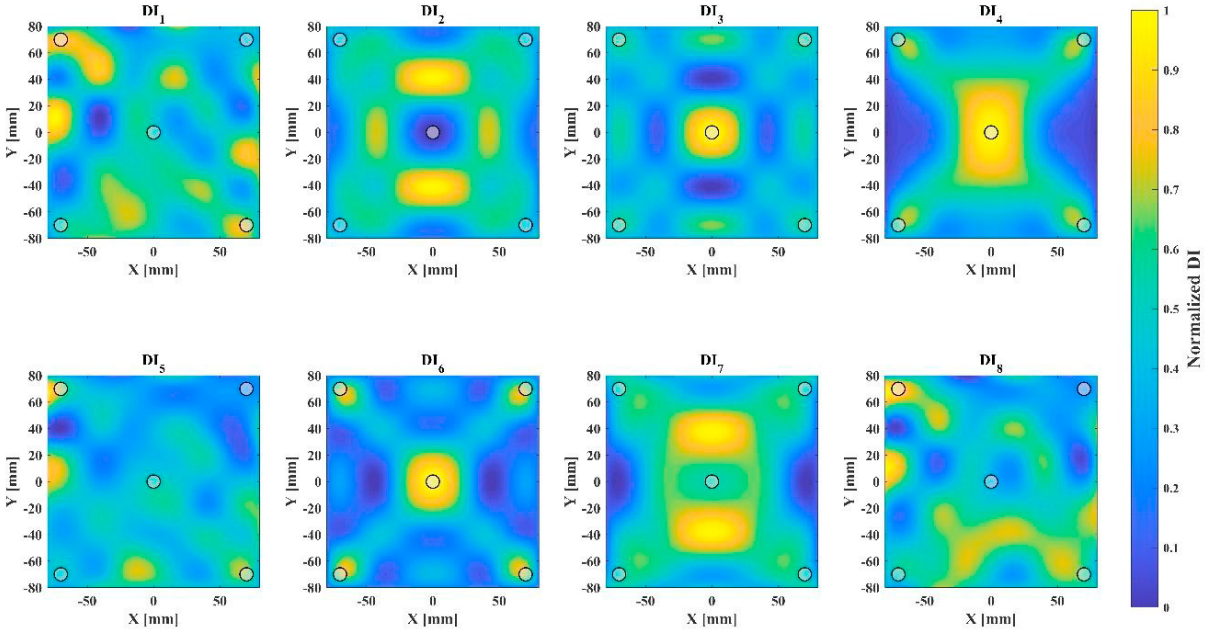

Fig. 2. Spatial sensitivity of the considered DIs.

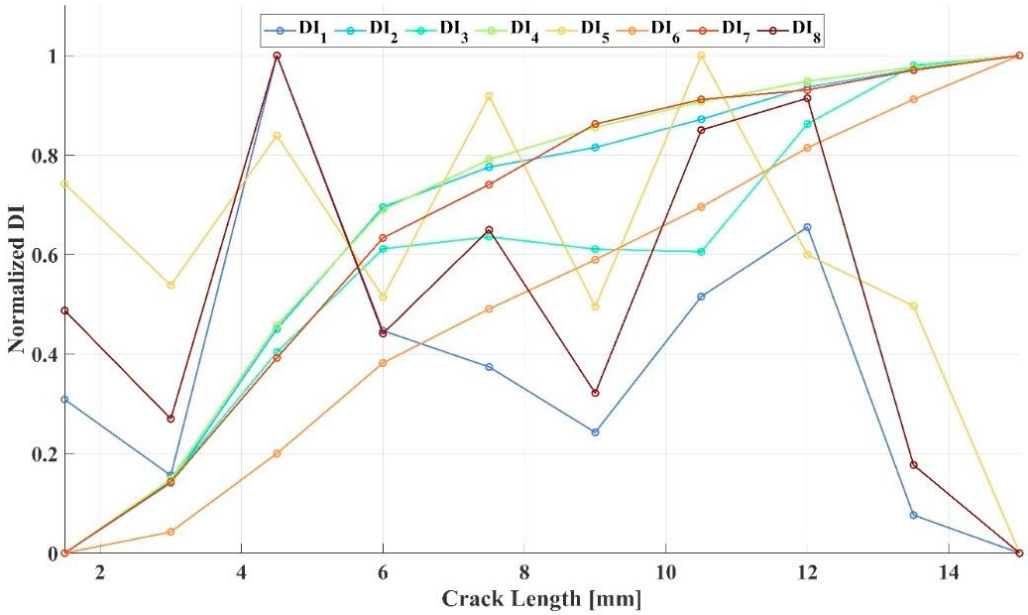

Fig. 3. Crack length vs. DIs.

Table 2. LES and PES of all considered DIs.

	DI_1	DI_2	DI_3	DI_4	DI_5	DI_6	DI_7	DI_8
LES	0.095	0.858	0.905	0.850	0.211	0.991	0.88	0.063
PES	0.109	0.401	0.249	0.448	0.095	0.29	0.45	0.096

4. Conclusions

This study presented an evaluation of eight DIs for UGW-based SHM, using finite element simulations of a cracked aluminum panel. A series of numerical experiments were conducted to systematically assess the effectiveness of each DI in capturing both the presence and progression of damage, as well as its spatial location. The results revealed significant variability in the performance of the indices. DI_6 and DI_3 exhibited the highest sensitivity to crack length, with LES of 0.991 and 0.905 respectively, indicating a strong monotonic relationship between their values and the crack growth. In terms of spatial coherence, DI_7 and DI_4 reached the highest PES, suggesting a strong correlation between their responses and the proximity to the receivers. While DI_2 demonstrated a balanced performance across both criteria (LES = 0.858, PES = 0.401), other indices such as DI_1 and DI_8 showed limited effectiveness, with low scores in both cases. These findings reinforce the notion that DIs should not be universally applied without consideration of the specific structural configuration, damage characteristics, and signal behavior. Future developments will also aim to classify the DIs based on their sensitivity to model parameters, thereby identifying indices that are not only effective but also robust to variations in the simulation setup or real-world operating conditions.

References

De Luca, A., Perfetto, D., Lamanna, G., Aversano, A., & Caputo, F. (2021). Numerical Investigation on Guided Waves Dispersion and Scattering Phenomena in Stiffened Panels. *Materials*, *15*(1), 74.

De Luca, A., Perfetto, D., Polverino, A., Aversano, A., & Caputo, F. (2022). Finite Element Modeling Approaches, Experimentally Assessed, for the Simulation of Guided Wave Propagation in Composites. *Sustainability (Switzerland)*, *14*(11).

De Luca, A., Perfetto, D., Polverino, A., Minardo, A., & Caputo, F. (2023). Development and validation of a probabilistic multistage algorithm for damage localization in piezo-monitored structures. *Smart Materials and Structures*.

Hu, M., He, J., Zhou, C., Shu, Z., & Yang, W. (2022). Surface damage detection of steel plate with different depths based on Lamb wave. *Measurement: Journal of the International Measurement Confederation*, *187*.

Konstantinidis, G., Drinkwater, B. W., & Wilcox, P. D. (2006). The temperature stability of guided wave structural health monitoring systems. *Smart Materials and Structures*, *15*(4).

Özgan, K., Şimşek, S., & Kahya, V. (2024). Automated damage assessment in truss structures via FE model updating and teaching-learning-based optimization. *Journal of Structural Engineering & Applied Mechanics*, *7*(4), 219–237.

Su, Z. (Zhongqing), & Ye, L. (Lin). (2009). *Identification of damage using Lamb waves : from fundamentals to applications*. Springer.

Wang, X., Dai, W., Xu, D., Zhang, W., Ran, Y., & Wang, R. (2020). Hole-edge corrosion expansion monitoring based on lamb wave. *Metals*, *10*(11), 1–16.

Wu, J., Xu, X., Liu, C., Deng, C., & Shao, X. (2021). Lamb wave-based damage detection of composite structures using deep convolutional neural network and continuous wavelet transform. *Composite Structures*, *276*.